Investigation of Fickian diffusion in the ternary mixture of 1,2,3,4-tetrahydronaphthalene, isobutylbenzene, and dodecane

A. Mialdun,[1] V. Sechenyh,[1] J. C. Legros,[1] J. M. Ortiz de Zárate,[2] and V. Shevtsova[1,a)]
[1]*Microgravity Research Center, Université Libre de Bruxelles (ULB), CP–165/62, Av. F. D. Roosevelt, 50, B–1050 Brussels, Belgium*
[2]*Departamento de Física Aplicada I. Universidad Complutense, Madrid, Spain*

(Received 20 April 2013; accepted 21 August 2013; published online 10 September 2013)

We present a comprehensive analysis of experimental results obtained for Fickian diffusion in the benchmark ternary liquid mixture of 1,2,3,4-tetrahydronaphthalene, isobutylbenzene, and dodecane (nC_{12}) with equal mass fractions. Isothermal diffusion coefficients have been measured by two independent experimental methods: by Taylor dispersion technique, and by a counter flow cell fitted with an optical interferometry device. The experimental diffusion matrices have been critically analyzed regarding the Onsager reciprocal relations, for which we introduce a matrix asymmetry index s^2 that is independent of the frame of reference and the component order. © *2013 AIP Publishing LLC*. [http://dx.doi.org/10.1063/1.4820357]

I. INTRODUCTION

Molecular diffusion in fluids is essential for a wide range of physical and chemical processes. Important examples include chemical and electrochemical reactions, crystal growth and dissolution, distillation, absorption, extraction, and transport across membranes. Nowadays, robust experimental techniques have been developed for the measurement of diffusion in binary mixtures, and reliable experimental data exist for many of these systems. But the liquids appearing in nature and in industrial applications are essentially multicomponent, a fact that leads research focus to move lately to diffusion in multicomponent liquid systems, starting with ternary mixtures.[1–10] However, mainly due to experimental and mathematical difficulties, even in ternary mixtures, diffusion coefficients are so far available only for a very limited number of these systems. Furthermore, in those cases where more than one data exist, quite often measurements by different experimental groups or by different techniques do not agree.[3,11,12] In addition to obvious industrial applications, reliable experimental data on multicomponent diffusion are needed for elucidating some fundamental questions still under discussion, like (a) whether the eigenvalues of the diffusion matrix of a ternary mixture are pseudo-binary diffusion coefficients;[13] or (b) whether main diffusion coefficients, D_{11} and D_{22}, in ternary mixtures are always positive or not.[14]

Our current interest in examining diffusion in multicomponent systems is also motivated by its utility for the interpretation of thermal diffusion (also called Soret, or thermodiffusion) experiments. Thermal diffusion effect is concentration separation in a liquid mixture as a response to the imposition of a thermal gradient. Measurements of thermal diffusion in binary mixtures are well established,[15,16] but the case of multicomponent (even ternary) mixtures poses serious difficulties both from the experimental and the mathematical sides. The later difficulties appear in the fitting of the experimental data to a mathematical model of the experiment, related to the large number of unknown parameters to be extracted. Prior knowledge of mass diffusion coefficients can dramatically decrease the complexity of the determination of thermodiffusion coefficients. Of course, the difficulties associated with having to extract many parameters from fitting a limited set of experimental data also exist in isothermal diffusion in multicomponent mixtures,[11,17] and indeed this will be a main theme of the current paper. Addressing these problems is the somewhat simpler case of isothermal diffusion that will eventually help future work in thermal diffusion. Regarding thermodiffusion in ternary mixtures, it is worth mentioning that in the frame of European Space Agency (ESA) microgravity program, the science team is currently performing DCMIX (Diffusion and Thermodiffusion Coefficients Measurements in Ternary Mixtures) experiment onboard the International Space Station (ISS),[18] where microgravity conditions make it possible to perform measurements that otherwise are not possible on earth. Thorough investigation of (isothermal) diffusion will undoubtedly benefit these (and others) thermal diffusion experiments. In any case, the problem with diffusion data for thermodiffusion experiments is that they have to be known with very high precision.

For all the above reasons, we have conducted and presented in this paper versatile isothermal diffusion measurements for a specific ternary mixture that is considered nowadays as a benchmark for ternary thermal diffusion in hydrocarbons: 1,2,3,4-tetrahydronaphthalene (THN), isobutylbenzene (IBB), and dodecane (nC_{12}), with equal mass fractions of components.[8,9] To obtain a highly reliable set of data, we employed two independent experimental techniques of different physical nature. Namely, Taylor dispersion technique (TDT) and digital interferometry applied to a classical diffusion cell by the principle of creating an

a)Author to whom correspondence should be addressed. Electronic mail: vshev@ulb.ac.be

interface, which we will refer later on as Counter Flow Cell (CFC). To further the reliability of the reported data, we discuss the Onsager symmetry that has to verify the diffusion matrix, and that we somewhat use as a guide to select the right diffusion matrix.

This paper is organized as follows: in Sec. II we review the theoretical basis of the experimental techniques, and we introduce a matrix asymmetry index as a useful tool to quantify deviations from the Onsager reciprocal relations, independently of the component order or the frame of reference. Section III is devoted to the details of our two different experimental setups and to the analysis of experimental data. Then, in Sec. IV, the attention is focused on the mathematical fitting details for each one of the two techniques evaluated. Next, in Sec. V, our current results are compared with available literature data. Finally, conclusions are given in Sec. VI.

II. THEORY

A. Theoretical approach

We consider a ternary mixture, where two concentrations c_1 and c_2 are chosen as independent. If we denote the mass fraction of component i by c_i, so that $c_1 + c_2 + c_3 = 1$, the two independent mass diffusive fluxes, $\mathbf{J}_1$ and $\mathbf{J}_2$, can be written as[19]

$$\mathbf{J}_1 = -\rho D_{11}\nabla c_1 - \rho D_{12}\nabla c_2, \tag{1}$$

$$\mathbf{J}_2 = -\rho D_{21}\nabla c_1 - \rho D_{22}\nabla c_2, \tag{2}$$

where D_{ij} are the diffusion coefficients in the center of mass frame of reference, and ρ the mass density of the mixture. In this paper, we prefer to adopt the mass frame of reference for diffusion because it best combines with the Navier-Stokes equations (balance of momentum). In what follows, the transport coefficients are assumed to be constant and correspond to a (uniform) temperature T_0 and to a reference composition, $c_0 = (c_{10}, c_{20})$, representative of the range in which concentrations vary. The third diffusive flux, $\mathbf{J}_3$, is defined from the condition that the fluxes of all components must sum up to zero.

If the liquid mixture is quiescent, mass conservation requires

$$\frac{\partial c_i}{\partial t} = -\nabla \cdot \mathbf{J}_i,$$

then the governing equations are

$$\frac{\partial c_1}{\partial t} = D_{11}\nabla^2 c_1 + D_{12}\nabla^2 c_2, \tag{3}$$

$$\frac{\partial c_2}{\partial t} = D_{21}\nabla^2 c_1 + D_{22}\nabla^2 c_2. \tag{4}$$

The solution of this system of equations has to take into account the geometry of the problem, through appropriate boundary and initial conditions, that will be detailed below when separately discussing each experimental technique. Here we simply underline that, regardless of the experimental method, the temporal evolution of the solution to Eqs. (3) and (4) will take the form of two series of exponentials:

$$c_1(t) = c_{10} + A_1 \sum_{m=0}^{\infty} \alpha_{1,m} \exp\left(-\tilde{\alpha}_m \hat{D}_1 t\right) + A_2 \sum_{m=0}^{\infty} \alpha_{2,m} \exp\left(-\tilde{\alpha}_m \hat{D}_2 t\right), \tag{5a}$$

$$c_2(t) = c_{20} + A_3 \sum_{m=0}^{\infty} \alpha_{1,m} \exp\left(-\tilde{\alpha}_m \hat{D}_1 t\right) + A_4 \sum_{m=0}^{\infty} \alpha_{2,m} \exp\left(-\tilde{\alpha}_m \hat{D}_2 t\right), \tag{5b}$$

where $\tilde{\alpha}_m$ and A_i are constants, $\hat{D}_1$ and $\hat{D}_2$ are the eigenvalues of the diffusion matrix

$$\hat{D}_1 = \tfrac{1}{2}\left(D_{11} + D_{22} + \sqrt{(D_{11} - D_{22})^2 + 4D_{21}D_{12}}\right), \tag{6a}$$

$$\hat{D}_2 = \tfrac{1}{2}\left(D_{11} + D_{22} - \sqrt{(D_{11} - D_{22})^2 + 4D_{21}D_{12}}\right), \tag{6b}$$

and the functions $\alpha_{i,m}(\mathbf{r})$ contain the spatial dependence. The working equations for each experimental technique are derived from Eqs. (5a)–(6b), using suitable physical quantities (voltage, refractive index, etc.), and finding the $\alpha_{i,m}(\mathbf{r})$ functions and constants, $\tilde{\alpha}_m$ and A_i, to solve the spatial part while verifying the appropriate boundary and initial conditions. To finalize this paragraph, we remind that the eigenvalues of the diffusion matrix have the same numerical value, independent of whether the diffusion matrix is expressed in the mass frame of reference or in the volume frame of reference.[19]

In this paper, we will be dealing with the inverse problem, i.e., to determine the matrix D_{ij} that best explains a given experimental output. This process is very demanding and it involves the notoriously difficult problem of determining the parameters of a multi exponential decay. In practice, to determine experimentally the transport coefficients D_{ij}, it will be necessary to minimize the sum

$$\Phi = \sum_i \left\{ f_{\text{exp}}(t_i) - f_{\text{calc}}\left[c_1(t_i), c_2(t_i)\right]\right\}^2 \tag{7}$$

of the squared differences between the measured values of some physical quantity f_{exp} and its values f_{calc} calculated from a theoretical model of the experiment based on Eqs. (5a)–(6b).

B. Onsager reciprocal relations

As it is well known,[19,20] the Onsager reciprocal relations, when applied to isothermal, multicomponent diffusion, demand the symmetry of the phenomenological matrix that connects mass fluxes to chemical potential gradients. The experimentally accessible diffusion matrix D is related to the Onsager matrix L by[19,20]

$$\mathsf{D} = \frac{1}{\rho T_0}\mathsf{L}\mathsf{G}, \tag{8}$$

where G is the equation of state (EOS) matrix of derivatives of chemical potential differences,

$$G_{ij} = \left(\frac{\partial \hat{\mu}_i}{\partial c_j}\right)_T, \tag{9}$$

with $\hat{\mu}_i = \mu_i - \mu_n$, the difference between the chemical potential of the i component of the mixture and the last one (solvent), whose concentration is taken as dependent variable. From Maxwell thermodynamic relations, it follows that the matrix G is symmetric, $G_{12} = G_{21}$ in the case of a ternary mixture. Notice that in Eq. (8) we adopt the definition of the Onsager matrix as in the book by de Groot and Mazur,[20] which is the inverse of the Onsager matrix H as defined by Taylor and Krishna.[19] Independently of the definition one adopts of the Onsager matrix, it has to be symmetric, $\mathsf{L} = \mathsf{L}^{\mathsf{T}}$. In the case of a ternary mixture, in view of Eq. (8), the symmetry property leads to a single relationship,

$$-G_{11}D_{12} + G_{12}D_{11} = -G_{22}D_{21} + G_{21}D_{22}, \tag{10}$$

which is an exact thermodynamic equation that must be verified for any system at any composition or temperature.[19,20] We stress that Eq. (10) is valid in both the mass frame of reference and the molar frame of reference. In the mass frame of reference, the chemical potentials in the definition (9) of the EOS matrix are specific (per unit mass) and the derivatives are with respect to concentrations in mass fraction. In the molar frame of reference, the chemical potentials in the definition (9) of the EOS matrix are per mole and the derivatives are with respect to concentrations in molar fraction. It can be demonstrated that if Eq. (10) is satisfied in the mass frame of reference, the equivalent expression is automatically satisfied in the molar frame of reference. Due to experimental uncertainties, the Onsager condition of Eq. (10) is not verified exactly for most of the available literature data.[11]

The practical use of Eq. (10) in diffusion research requires the knowledge of the EOS of the mixture. Unfortunately, reliable EOS data published in referred journals for our particular ternary system (THN-IBB-nC_{12}) are not available. Hence, we assume this system to be an ideal mixture that is expected to be a good first approximation for this hydrocarbon mixture, which, at the temperature of interest, does not exhibit phase separation in the whole range of composition. Adopting such an approximation, one has

$$\begin{aligned}\hat{\mu}_1 &= \frac{RT}{M_1}\ln x_1 - \frac{RT}{M_3}\ln(1-x_1-x_2),\\ \hat{\mu}_2 &= \frac{RT}{M_2}\ln x_2 - \frac{RT}{M_3}\ln(1-x_1-x_2),\end{aligned} \tag{11}$$

where M_1, M_2, and M_3 are the molar masses of, respectively, THN, IBB, and nC_{12}; R is the gas constant. Symbols x_i represent the concentrations in mole fraction, $x_3 = 1 - x_1 - x_2$. From Eq. (11), one readily obtains for the EOS matrix G in the mass frame of reference,

$$\mathsf{G} = \frac{RT}{M_3 x_3}\begin{bmatrix} 1 + \dfrac{M_3 x_3}{M_1 x_1} & 1 \\ 1 & 1 + \dfrac{M_3 x_3}{M_2 x_2}\end{bmatrix} \cdot \mathsf{P}, \tag{12}$$

where $P_{ij} = (\partial x_i/\partial c_j)$ is the matrix of concentration derivatives. For a ternary mixture, it is conveniently expressed as[19]

$$\mathsf{P} = \begin{bmatrix} x_1\left(\dfrac{x_3}{c_3} + \dfrac{1-x_1}{c_1}\right) & x_1\left(\dfrac{x_3}{c_3} - \dfrac{x_2}{c_2}\right) \\ x_2\left(\dfrac{x_3}{c_3} - \dfrac{x_1}{c_1}\right) & x_2\left(\dfrac{x_3}{c_3} + \dfrac{1-x_2}{c_2}\right)\end{bmatrix}. \tag{13}$$

The Hessian P is the same matrix appearing when changing a diffusion matrix from mass frame of reference to molar frame of reference: $\mathsf{D}_x = \mathsf{PDP}^{-1}$, where D_x is the diffusion matrix in the molar frame of reference.

For the particular case that interests us here, the symmetric point of the mixture THN-IBB-nC_{12} (i.e., equal mass fractions), the molar fractions are $x_1 = 0.3622$ and $x_2 = 0.3567$. Using the molecular mass values of the chemical species, we obtain from Eqs. (12) and (13),

$$\mathsf{G} = RT\begin{bmatrix} 3.9892 & 1.7228 \\ 1.7228 & 3.9606\end{bmatrix} \times 10^{-2}, \tag{14}$$

that, as anticipated, is a symmetric matrix. The matrix G given by Eq. (14) is what we actually use in the experimental section, Sec. IV.

C. Degree of asymmetry of a matrix

As it will be further elaborated below, it is in general difficult to extract the diffusion matrix from experiments. This is due to a combination of reasons like ill-conditioned fitting procedures,[17] contrast factors leading to bad condition numbers,[21] signals of very small amplitude.[11] Hence, one possible practical use of Onsager relations, Eq. (10) for ternary mixtures, is as a guide to select the "best" diffusion matrix among a pool of possible ones. For such a purpose, we need an index to measure how symmetric the matrix DG^{-1} is. For the case of ternary mixtures, Spera and Trial[22] or Firoozabadi[2] proposed to simply evaluate (in %) the difference between the right-hand and left-hand sides of Eq. (10). Namely, introducing notation,

$$F_1 = -D_{12}G_{11} + G_{12}D_{11}, \quad F_2 = -D_{21}G_{22} + G_{21}D_{22},$$

the asymmetry of the phenomenological matrix DG^{-1} would be defined as

$$\delta_{\mathrm{Ons}}(\%) = 100\%\frac{2(F_1 - F_2)}{(F_1 + F_2)}. \tag{15}$$

However, the practical use of Eq. (15) as a consistency test for a given set of measurements, or to compare the quality of various experimental data sets, is compromised by the fact that the numerical value of the quantity δ_{Ons} depends on the frame of reference and on the ordering of the components when enumerating the mixture (see Sec. V). Furthermore, it cannot be

obviously generalized from ternary to multicomponent mixtures. Therefore, it would be very valuable to have an alternative method to quantitatively asses how well a given data-set verifies Onsager relations, and whose outcome were independent of the component order and of the frame of reference, and that can be readily generalized for multicomponent mixtures. For this purpose, we found useful the Hammond's definition of the degree of asymmetry of a given matrix.[29,30] Since this asymmetry index is not well-known outside the mathematics literature, we briefly review its definition here, and some of its more relevant properties for our current purposes.

Let us consider an arbitrary matrix H and let us try to "measure" how symmetric it is. For such a goal, let us first compute

$$\mathsf{S} = \frac{1}{2}[\mathsf{H} + \mathsf{H}^{\mathsf{T}}] \tag{16}$$

that is a symmetric matrix by construction. Then, the Hammond's degree of asymmetry s^2 of the original matrix H is defined as[29,30]

$$s^2 = \det(\mathsf{S}^{-1/2}\mathsf{H}\,\mathsf{S}^{-1/2}). \tag{17}$$

It can be demonstrated that s^2 is well-defined if the eigenvalues of H are real and positive, which is the case here since we plan to apply this definition to an Onsager matrix, the product DG^{-1}. The asymmetry s^2 is a number between 1 and 2. For a symmetric matrix H, $s^2 = 1$. The closer is s^2 to 1, the more symmetric the original matrix H is. The closer s^2 to 2, the more asymmetric the original matrix H is. The degree of asymmetry s^2 of a matrix is independent of the coordinate system used to represent it. We refer to the specialized mathematics literature[29,30] for a detailed discussion of these features.

For the application of this definition to diffusion in multicomponent systems, we remark the following: First, s^2 is a dimensionless quantity. Second and most important, for given diffusion and EOS matrices, the degree of asymmetry s^2 of the product DG^{-1} is independent of the order in which components are listed, or of the frame of reference, whether mass or molar. These two important properties are independent of the number of components of the mixture (the dimension of the matrices D and G).

To obtain the Hammond's degree of asymmetry s^2 of a given DG^{-1}, one has to evaluate the square root of a matrix, as required by Eq. (17). For mixtures with a large number of components, such a computation can be, in general, difficult. However, for the case we are dealing with here of a ternary mixture, there exists a relatively simple algorithm that gives one of the square roots of an arbitrary 2×2 matrix S, namely,

$$\mathsf{S}^{1/2} = \frac{1}{\sqrt{\mathrm{tr}\mathsf{S} + 2\det \mathsf{S}}}\left[\mathsf{S} + \sqrt{\det \mathsf{S}}\begin{pmatrix} 1 & 0 \\ 0 & 1 \end{pmatrix}\right], \tag{18}$$

a formula that can be easily verified by simple substitution or numerically. Of course, there are more square roots of S (up to four for 2×2 matrices) that can be computed by variations in some signs in the formula above. The resulting Hammond's degree of asymmetry s^2 is independent, of which one of the square roots is selected. In the calculations presented later, Eq. (18) is used.

In summary, we have a method to measure by a single number (s^2) how close to symmetric a matrix is, that can be used to asses how well a given experimental data set verifies the Onsager reciprocal relations (Eq. (10) for a ternary mixture). The value of s^2 for a given experimental data set is independent of the order in which the components of the mixture are listed or of whether mass or molar frame of references are employed. This s^2 index has clear advantages over the δ_{Ons} index proposed by other authors.[2,22] We shall apply to our experimental results the "Onsager quality test" that consists in evaluating both δ_{Ons} and Hammond's s^2 degrees of asymmetry of the product DG^{-1}. For G, lacking more specific information, we shall use the ideal approximation of Eq. (12).

III. EXPERIMENTAL METHODS

A. Samples

All the measurements were performed with dodecane (Acros Organics, 99%), isobutylbenzene (Acros Organics, 99.5%), and 1,2,3,4-tetrahydronaphthalene (Acros Organics, more than 98%) without further purification. The liquid samples were degassed prior to the experiment.

B. Taylor dispersion technique (TDT): Experiment description

A widely used method for measuring mass diffusion coefficients is the Taylor dispersion technique. This technique has certain advantages: possibility of measurements over a wide range of temperature and pressure; it does not require a calibration procedure with a liquid of known diffusivity; and it is relatively simple in realization because the set-up consists of components available on the HPLC (High-performance liquid chromatography) market. Since the pioneering publications by Taylor[23] for binary mixtures, the theoretical approach has been extended for measuring mass diffusion in ternary[17,24,25] and even quaternary[26] liquid mixtures.

The experimental principle of TDT is the diffusive spreading of a small sample of mixture injected into a laminar flow of a carrier fluid with a slight concentration difference. Here, the carrier liquid is the ternary mixture at the (mass) symmetric point, so that the test liquid plays the role of carrier liquid as well. Our setup is schematically shown in Fig. 1(a), the perturbing solution is injected at the entrance of a long dispersion tube (29.839 ± 0.001 m), made of polytetrafluoroethylene (PTFE) with circular cross-section of radius $R = 374\,\mu$m. The flow of the carrier mixture is laminar with a constant flow rate of 0.079 ml/min. The direction of the flow is shown by arrows in Fig. 1(a). To prevent bubbles, which create disturbances in the flow and reduce the quality of the measurements, a SYSTEC degassing module is installed and connected in-line before the pump. The injected volume ($20\,\mu l$) of a mixture with slightly different concentrations, as

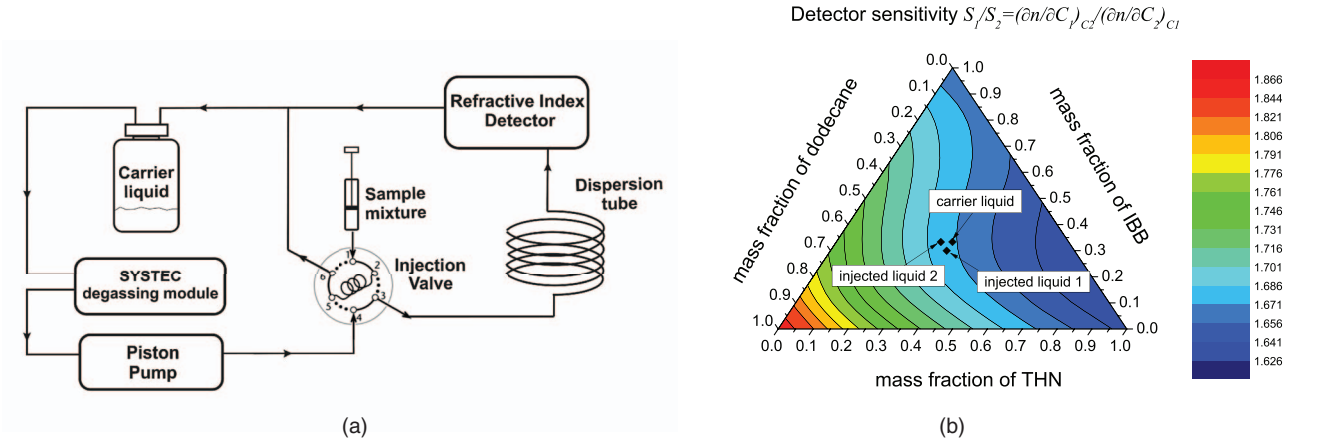

FIG. 1. (a) Sketch of the set-up used in Taylor dispersion technique. (b) Compositions of the injected samples on the triangle with isolines of the detector sensitivity ratio. The test liquid plays the role of career liquid as well.

it moves along the tube, is dispersed by the simultaneous effects of Poiseuille flow and radial molecular diffusion.

The concentration as a function of time is monitored at the end of the dispersion tube with a Knauer Smartline RI 2300 differential refractive index detector (RID), which is well suited for detecting small composition variations. An example of these signals (after baseline subtraction) is shown in Fig. 2(a). The sign of the signal is determined by the sign of Δn (difference of refractive indices between the carrier liquid and the injected sample) and is negative in our case. In Fig. 2(a), the absolute value of the signal is actually given. Figure 2(b) shows the level of background noise. Typical values of the base line noise were less than $\pm 5 \times 10^{-8}$ V. A detailed description of the experimental setup and its validation with binary mixtures can be found elsewhere.[27]

Ternary dispersion profiles are generated by injecting small samples of mixture containing components 1 and 2 with mass fractions $(c_{10} + \delta c_1)$ and $(c_{20} + \delta c_2)$ into the carrier stream of composition c_{10} and c_{20}. Actually, in this paper, the mixture THN-IBB-nC$_{12}$ with equal mass fractions of the components $c_{i0} = c_0 = 1/3$ is analyzed. The application of TDT to ternary mixtures allows to select any two concentration differences δc_i among the three possible for injection. To ensure the most favorable conditions for conducting the diffusion measurements in the THN-IBB-nC$_{12}$ mixture, we selected the initial concentration gradients in the components for which the detector sensitivity ratio $S_1/S_2 = (\partial V/\partial c_1)_{c_2}/(\partial V/\partial c_2)_{c_1}$ is larger. This ratio is proportional to the ratio of the optical contrast factors $S_1/S_2 \sim S_{\text{opt}} = (\partial n/\partial c_1)_{c_2}/(\partial n/\partial c_2)_{c_1}$. Concentration derivatives of the refractive index $(\partial n/\partial c_i)$ for our mixtures can be estimated using available literature data,[28] from which we adopted the tabulated values at wavelength $\lambda = 925$ nm, which is closer to the wavelength of the light source of our RI detector ($\lambda = 950$ nm). We conclude that the ratio of optical factors S_{opt} at the symmetric point is larger for the components THN and IBB. Hence, they are selected in TDT for initial concentration gradients. For reference, the isolines of detector sensitivity ratio S_{opt} are shown by background colors in Fig. 1(b).

The two injected samples had compositions, which are close to the carrier (test) liquid. The compositions of the carrier liquid and injected samples are shown in Fig. 1(b). The

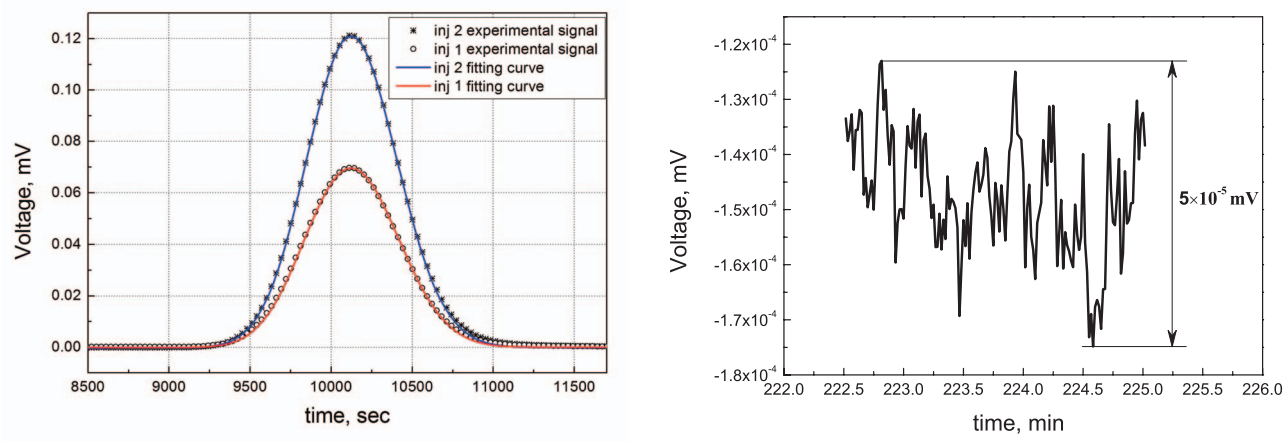

FIG. 2. (a) Absolute value of ternary dispersion profiles (symbols) and fitting curves in ternary mixture THN-IBB-nC$_{12}$ with equal mass fractions at 298.15 K; "inj 1" and "inj 2" stand for "injection sample 1" or "injection sample 2," respectively. (b) A typical level of background noise in base line (at the end of the curve in the left plot).

first sample creates the initial concentration difference in IBB which is equal to $\delta c_2 = 0.03365$. The second sample creates the initial concentration difference in THN which is equal to $\delta c_1 = 0.03238$. Thus, the working mixtures are:

- Carrier liquid: $c_0/c_0/c_0$.
- Injected sample (1): $c_0/(c_0 - \delta c_2)/(c_0 + \delta c_2)$.
- Injected sample (2): $(c_0 - \delta c_1)/c_0/(c_0 + \delta c_1)$.

Each of these samples was injected into the carrier liquid at least two times and, correspondingly, four different experimental signals are available for the procedure of extraction of mass diffusion coefficients.

C. Taylor dispersion technique (TDT): Analysis of signals

The signals in Fig. 2(a) show that the initial sharp pulse of concentration is stretched into a shape whose theoretical modeling we discuss below.[23–25] The diffusion coefficients are then extracted by fitting the experimentally measured signals to these theoretical expressions.[17] Using the RI detector sensitivities S_1 and S_2 with respect to components 1 and 2 (introduced in Sec. III B), an equation for the raw signal can be written as[17,24]

$$V(t) = V_\infty + V_1 t + S_1[c_1(t) - c_{10}] + S_2[c_2(t) - c_{20}]. \quad (19)$$

The two first terms $(V_\infty + V_1 t)$ take into account a drift of the base line, and they have to be subtracted from the raw signals.

After background subtraction, we first analyze the quality of signals. Indeed, before performing any detailed modeling and as part of the selection routine, some (model-independent) characteristics of the signals were determined, and are listed in Table I for the four runs considered in this paper. The plots in Figure 2(a) corresponded to the signals #1 and #3 in Table I. We observe that all signals display a single maximum at a retention time t_R. The peak height $\Delta V_{\max}$ at the maximum ($t = t_R$) depends on the composition of the injected sample. Values of t_R and $\Delta V_{\max}$ are listed in the second and third columns of Table I, while the fourth column reports the corresponding signal surface area. Notice that retention time t_R is almost the same for all the injections, which indicates good stability of the flow rate of the carrier fluid. Comparison of the surface area values for all the experimental signals for the same injection sample also indicates good repeatability during measurements.

TABLE I. Characteristics of the signals obtained by TDT in the THN-IBB-nC_{12} mixture with equal mass fractions of each component.

Signal number	t_R (s)	$\Delta V_{\max}$ (mV)	Area (mV s)	D_{app} $\times 10^{-10}$ (m^2/s)	Skewness	Kurtosis
1	10128	−0.0661	48.14	6.98	2.233	6.626
2	10127	−0.0658	48.00	6.96	2.231	6.620
3	10126	−0.116	81.03	7.68	2.316	7.042
4	10127	−0.116	80.95	7.66	2.314	7.029

To report on the variance (width) of the signals, at this preliminary stage of data processing, we performed signal fittings considering the ternary mixture as if it were binary, i.e., using the original Taylor equations.[23] This process provides "apparent" diffusion coefficients (D_{app}) which are also listed in Table I. In this procedure, the non-essential for fitting long zero line is cropped out on both sides of the peak, symmetrically with respect to $t = t_R$. The number of points, N, retained on both sides of $t = t_R$ is increased up to the moment when D_{app} becomes independent of N, usually it is about $N \sim 3500$. The D_{app} give an idea about the values of the main coefficients of the diffusion matrix (D_{11} and D_{22}), and they will be used later on as initial guesses for the full nonlinear least-squares fitting algorithm. The calculation of pseudobinary diffusion coefficients from ternary measurements is justified in our case, as only one symmetric peak emerges, see Fig. 2(a). In the case of multiple peaks, the criteria of D_{app} and its use as initial guess are no longer available.[31]

Skewness is a measure of the asymmetry. The experimental values of signal skewness are reported in Table I. They are similar for all the peaks, about 2.3, which identify reasonably good symmetry with a possible small distortion in tails. Kurtosis is a measure of whether the data are peaked or flat relative to a normal distribution. From a normal probability function to a double exponential distribution, it ranges from 3 to 6. The measured kurtosis values in Table I display small variation in the range 6.6–7.

Not all the performed experimental runs are passed to the full non-linear fitting procedure. The preliminary thorough selection of the signals here described was not performed in our first experiments,[27] and it led to the different, less reliable, diffusion coefficients.

For the full non-linear fitting of the signals as required to obtain the diffusion coefficients D_{ij}, we used analytical solutions for $c_1(t)$, $c_2(t)$ from the literature,[17,24] adapted for the boundary and initial conditions appropriate to TDT. Substitution into Eq. (19) of these theoretical expressions[17,24] gives the basic equation for the detector signal:

$$V(t) = V_\infty + V_1 t + \Delta V_{\max}\sqrt{\frac{t_R}{t}}[W_1 \exp(-\hat{D}_1\eta) + (1 - W_1)\exp(-\hat{D}_2\eta)], \quad (20)$$

where W_1 (which is a function of D_{ij} and S_i) is a normalized weight, and $\eta = 12(t - t_R)^2/R_0^2 t$, with R_0 the tube radius. Hence, the detector signals for ternary diffusion resemble two superimposed Gaussian curves centered on the same retention time t_R. In practice, we had to adapt the original theory[17,24] to the use of mass fractions instead of molar concentrations. In a recent paper by Sechenyh *et al.*,[27] such an adaptation was presented, reporting an expression identical to Eq. (20), but where W_1 additionally depends on the molecular weights of the components. To close this section we finally mention that, as is well-known,[17,24] a single experiment (single run) in ternary mixtures does not provide enough data to obtain the full diffusion matrix, D_{ij}, so we always fit the experimental data to the mathematical model of Eq. (20) for a group of experiments simultaneously, at least one coming from the first

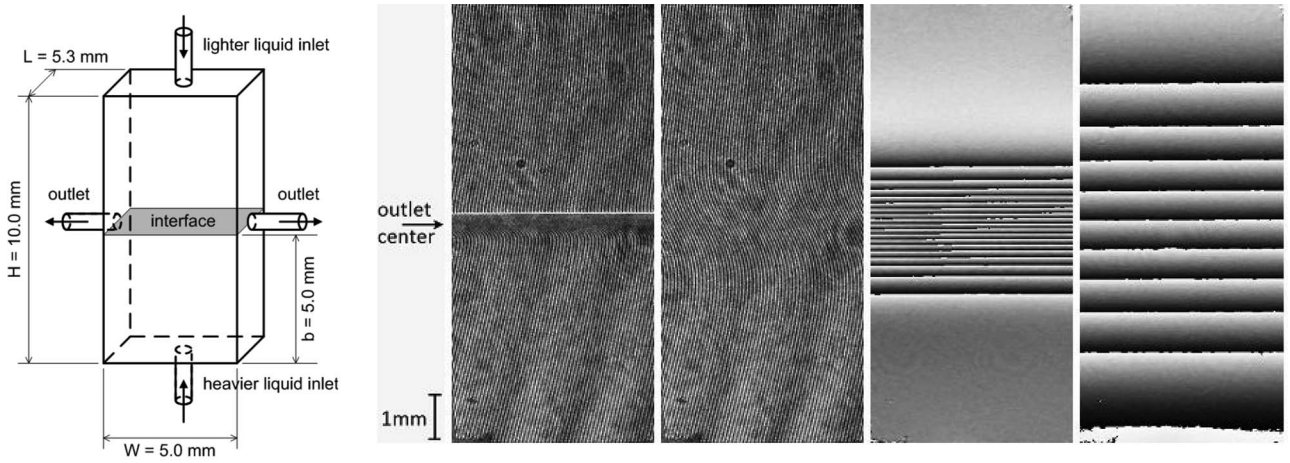

FIG. 3. (a) Sketch of the CFC cell. (b) Transient diffusion fields: first two pictures show fringe images at $t = 0$ min and $t = 5$ min, and the following two pictures show images of wrapped phase at $t = 5$ min and $t = 3$ h from the beginning of the experiment.

injection sample and another coming from the second injection sample.

D. Counter flow cell (CFC) method: Experiment description

For the measurements with a diffusion cell, we have chosen the counter flow method for creating an interface between two solutions of different but close concentrations. This method allows undemanding technical implementation, and, by proper manipulation, it provides an interface of fairly good sharpness. Indeed, different variations of this method have been successfully used for the measurement of mass diffusion coefficients in binary mixtures.[32] A sketch of the diffusion cell is shown in Fig. 3(a) where the principle of creating an interface is illustrated together with an indication of the characteristic dimensions of the cell. The body of the cell is made of a brass disk. A rectangular opening is cut in the disk, providing a volume to be filled with liquid. The disk is sandwiched between two optical windows with thin PTFE sheet seals isolating glass from metal. The design provides a geometric path for the probing beam in the bulk liquid of total length $L = 5.3$ mm. The whole set-up, including the cell, was maintained inside a thermally insulated box equipped with a system of active thermal control. The temperature inside the box was always kept at 298 K with residual fluctuations of less than ± 0.1 K. More details on the cell can be found elsewhere.[33]

At the beginning of each experimental run, a two-layer liquid system is formed inside the cell by the simultaneous injection of two solutions through the inlets, heavier mixture from bottom and lighter one from top. Since the concentrations differences are very small, the filling procedure requires a lot of attention. When the interface formation ends, the cell is closed and the experimental recording starts.

To examine the change in the refractive index of liquid within the cell, the classical Mach-Zehnder interferometer scheme is used. The light source is an expanded and collimated beam of a He–Ne laser with a wavelength of $\lambda = 632.8$ nm. The resulting interferogram is recorded by a CCD camera with a sensor of 1280×1024 pixels size. The resolution of the imaging system is around 60 pixels/mm. The interferometer has been aligned for a narrow fringe pattern and the extraction of optical phase has been implemented via 2D Fourier transform technique (see details elsewhere[34,35]). The image acquisition step has been varied from 10 s at the beginning of the experiment to 300 s at the end. The optical properties of the liquid mixtures needed for data extraction, namely, the derivatives of the refractive index at the working wavelength with respect to the two concentrations (so called contrast factors) have been taken from literature.[28]

The first two pictures in Fig. 3(b) show original fringe images for the experiment #2 (see Table II) corresponding to the variation of the refractive index at the time instants $t = 0$ min and $t = 5$ min. The first picture demonstrates that the interface shape is straight and even in case some 2D or 3D perturbations are present, they are squeezed into 0.5 mm thick boundary layer. The last two pictures in Fig. 3(b) show images of wrapped phase (as obtained by processing of fringe images) at the moments $t = 5$ min and $t = 3$ h. Note that wrapped phase map in the third picture is obtained from fringe image in the second picture.

The profile of the refractive index in vertical direction is a very symmetric function with respect to the interface location. This suggests that in the presented set of experiments there were no violation of buoyancy stability, and the diffusion coefficient does not vary significantly within the diffusion field.

E. Counter flow cell (CFC) method: Analysis of data

Four experiments, with slightly different initial composition differences between top and bottom layers, were analyzed. In three experiments, the concentration of one of the components was kept nearly constant and the other two were different, for example, $(c_{10} - \delta c)/(c_{20} + \delta c)/c_{30}$. Where the δc was taken with steps of $\delta c \sim \pm 0.01$ in mass fraction around the point of interest: mass fraction $c_{10} = c_{20} = 1/3$ for THN-IBB-nC_{12}. In one of the experiments (#4), the concentrations

TABLE II. Parameters of the experiments performed by the CFC technique.

	Experiment #1	Experiment #2	Experiment #3	Experiment #4
c_1^T	0.31996	0.34006	0.31998	0.31982
c_2^T	0.34001	0.31997	0.33998	0.32003
c_1^B	0.33891	0.33994	0.34002	0.33962
c_2^B	0.31991	0.34006	0.34007	0.33953
δc_1^{T-B}	− 0.01895	0.00012	− 0.02004	− 0.01980
δc_2^{T-B}	0.02010	− 0.02009	− 0.00009	− 0.01950
$\Delta n_{\text{calc}}^{(\text{m})} \times 10^4$	− 8.06	− 14.20	− 23.76	− 37.14
$\Delta n_{\text{exp}}^{(\text{m})} \times 10^4$	− 8.02	− 14.18	− 23.68	− 37.12
t_0 (s)	23.3	46.7	115	355
$D_{\text{app}} \times 10^{10}(\text{m}^2/\text{s})$	9.49	7.31	7.61	7.76

of all three components were different. The initial compositions used in the four experiments are listed in Table II. Concentrations of the top and the bottom solutions are marked as c_i^T and c_i^B, respectively, and $\delta c_i^{T-B} \equiv (c_i^T - c_i^B)$. Furthermore, these initial compositions are represented graphically in Fig. 4, where initial diffusion couples are linked with straight lines at magnified plot. Directions of major (1) and minor (2) eigenvectors are also represented in the same plot, which are built with the diffusion matrix extracted from these experiments following Thompson and Morral.[36] An effect of mutual orientation between eigenvector and particular diffusion couple will be shortly addressed below in Sec. IV C. Thus, the diffusion matrix at the composition of interest is derived from the simultaneous inversion of diffusion profiles in the four directions shown by straight lines. The 2%–4% difference in concentration between the two parts of the cell is a compromise between reducing the effect of the compositional dependence of the diffusion matrix and maintaining reasonably good analytical resolution of the concentration changes along the diffusion profile.

The maximum measured refractive index difference $\Delta n_{\text{exp}}^{(\text{m})}$ between the top and the bottom boundaries of the cell is given in Table II for the four runs analyzed. The evolution of $\Delta n(t)$ in time is shown in Fig. 5(a) for all the runs. Differences Δn between the upper and lower boundaries of the cell are associated not only to the difference in δc_i but also with the different values of the optical contrasts:[28] $(\partial n/\partial c_1)_{c2} = 0.118092$, and $(\partial n/\partial c_2)_{c1} = 0.070885$. The expected maximum refractive index difference is at $t = 0$, and can be estimated from the initial state of the system

$$\Delta n_{\text{calc}}^{(\text{m})} = \left(\frac{\partial n}{\partial c_1}\right)_{c_2} \delta c_1^{T-B} + \left(\frac{\partial n}{\partial c_2}\right)_{c_1} \delta c_2^{T-B}. \qquad (21)$$

The excellent agreement between the calculated and measured values of $\Delta n^{(\text{m})}$, both are given in Table II, proves that experimental data obtained with this new setup are consistent. Figure 5(b) shows a typical set of vertical profiles of refractive index obtained after processing of interferograms as function of time. The first profile at $t = 0.03$ h gives a hint about the interface sharpness.

The basic principle of extracting diffusion coefficients is to compare experimentally observed quantities (refractive index profiles, $n(z, t)$ in this case) with ones reconstructed from a mathematical model of the experiment, and tuning the mathematical model by varying the diffusion matrix to get the best match of both. In order to model the experiments, a solution of multicomponent diffusion equations based on the diffusion matrix diagonalization method[19,33] is used with proper initial and boundary conditions. Because the considered system

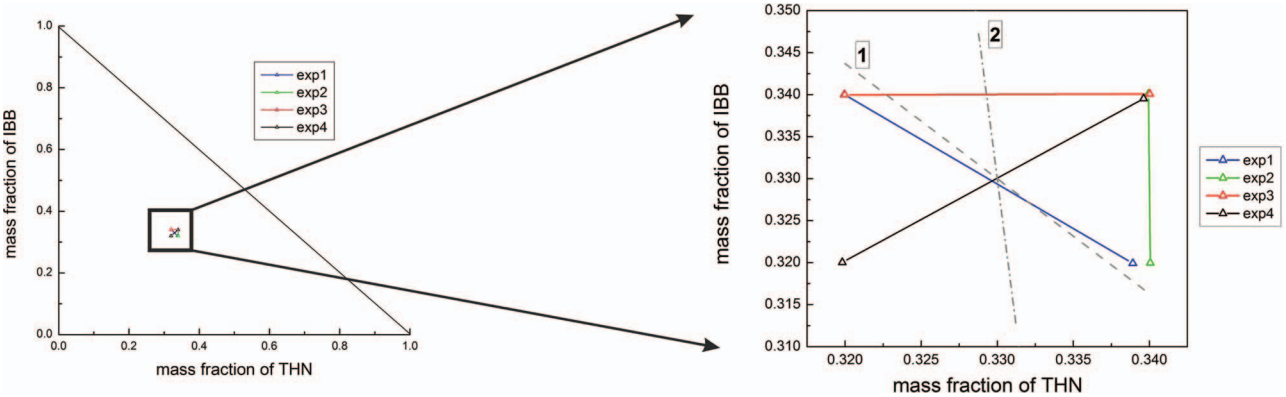

FIG. 4. Diffusion couples (initial concentrations in two parts of the cell) used in the experiments employing the counter flow cell technique for measuring diffusion coefficients at the symmetric point of the mixture THN-IBB-nC_{12}. Left plot shows the test points at the full concentration map, and right plot shows the magnified central region. Dashed lines indicate major (1) and minor (2) eigenvectors.

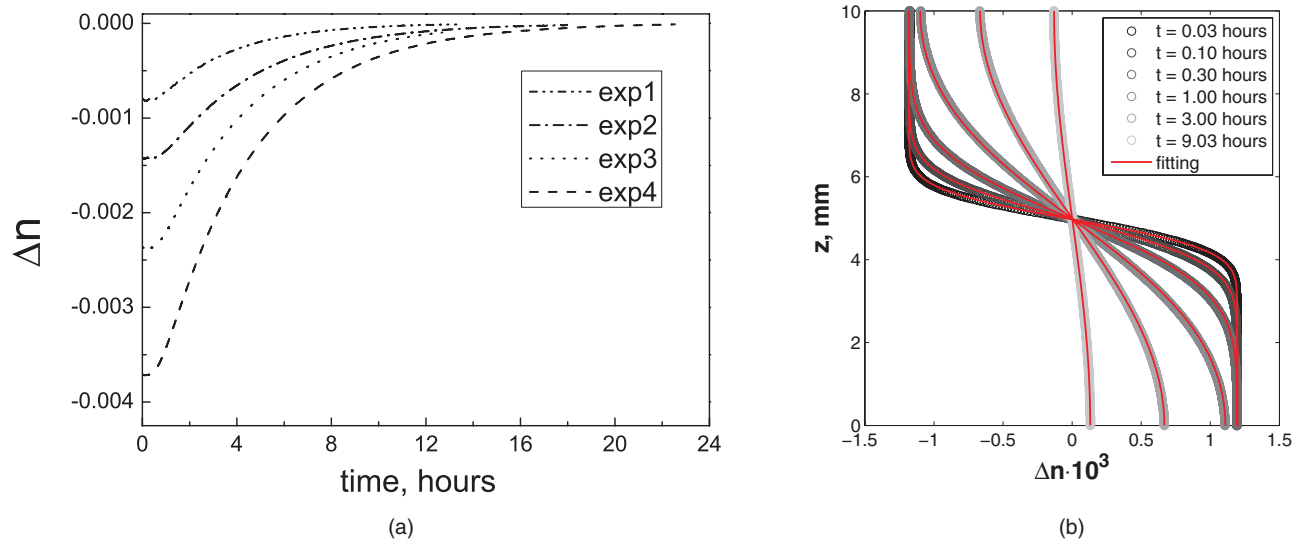

FIG. 5. (a) Temporal evolution of the refractive index difference between the top and the bottom of the cell, $\Delta n(t)$, in the different experiments. (b) Refractive index profiles $n(z, t)$ for the experiment #3 at different t values. The wide grey curves correspond to the experimental points, and the red curves are the result from the fitting.

is finite, the concentration fronts reach the cell boundaries in less than 1 h as clearly seen from Fig. 5(b), while the experiments last longer. Consequently, the conditions of zero mass flux must be imposed at the horizontal walls, and, as a result, the analytical solution is based on trigonometric functions.

The need to map the real experiment and the ideal theoretical model requires to minimize the level of imperfections affecting the experimental data. Certain shortcomings, specific to the CFC experiment, can be overcome with reasonable effort and are discussed next.

First, the initial distribution of the refractive index recorded in the experiment and naturally assigned to $t = 0$ does not have a perfect stepwise shape at the liquids interface, as it is supposed to be according to the analytical solution, see Fig. 5(b). This is a common problem for such type of experiments, and among the different approaches proposed in literature to treat it, we have chosen one based on introducing an initial time parameter t_0. This t_0 is the first time moment at which the theoretical profile coincides with the experimental profile. Parameter t_0 depends on the experiment development, and there is no way to estimate it *a priori*. For this reason we have always started with a preprocessing of each individual experiment, assuming a quasi-binary behavior with only two unknown fit parameters: t_0 and an apparent binary diffusion coefficient, D_{app}. This approach works well for this particular system as it does not demonstrate any unusual transport. Then, the initial time t_0 was assigned to each corresponding experimental data set, and the apparent diffusion coefficient was used in the next processing steps as initial guess. Values of both parameters for each experiment are also provided in Table II.

Second problem is related to the reference image needed for proper estimation of optical phase. Ideally, it should provide pure background with no trace of concentration change, which is difficult to achieve in practice. The presence of tiny undetectable concentration imperfections in the reference image can lead to data corruption, which will propagate over to the full data set. We found that the more reliable approach is to use the very last image of the experiment as reference. Figure 5(a) shows the temporal evolution of Δn in different experiments, and indicates that overall Δn^{T-B} vanishes practically for long enough experiments. Although, in some cases (like in experiment #3) the residual Δn can be noticeable. To be on safe side, we have established a way to eliminate the impact of any residual Δn, and have systematically implemented it for all experiments, regardless of their duration. The idea is to get rid of the very last calculated refractivity profile $n_{\text{calc}}(z, t_\infty)$, which has been implemented by slightly modifying the objective function that will take form:

$$\Phi = \sum_{i,j} [n_{\text{calc}}(z_i, t_j) - n_{\text{calc}}(z_i, t_\infty) - n_{\text{exp}}(z_i, t_j)]^2. \quad (22)$$

Application of these two corrections improves essentially the quality of the fit. Moreover, since our previous paper on this technique,[33] we have recognized and solved one more problem affecting the experimental data set. Now we have introduced and systematically applied a correction of refractive index profiles for optical path non-equality over the field of view of the diffusion cell. This optical non-uniformity is caused by a slightly non-uniform thickness of the PTFE seals, and can be evaluated interferometrically with no change of the experimental configuration. In spite of the smallness of this correction, and of the visually untraceable results of its application, fit results are affected dramatically. Indeed, the present results for diffusion coefficients differ from that presented previously.[33]

IV. EVALUATION OF THE DIFFUSION COEFFICIENTS

A. Fitting

As explained above, the experimental signals, $V(t)$ for TDT and $\Delta n(z, t)$ for CFC, are modeled by two working expressions: Eq. (20) for TDT and an expression of the type of

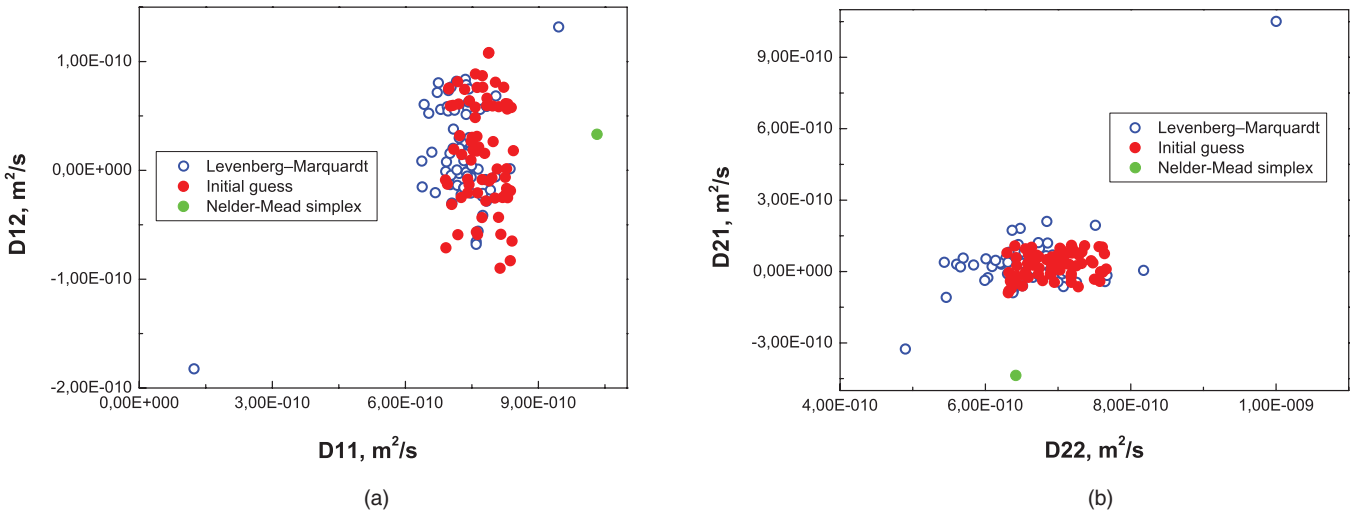

FIG. 6. Comparison of fit convergence using different algorithms. Red filled circles indicate 70 different initial guesses and blue circles show results of fitting using Levenberg-Marquardt algorithm. Green circle indicates results of fitting for the same initial guesses using Nelder-Mead (simplex) algorithm. Two diffusion couples are analyzed for experimental data from TDT: (a) (D_{11}, D_{12}); (b) (D_{22}, D_{21}).

Eqs. (5a) and (5b) for CFC. These theoretical models contain four unknown molecular diffusion coefficients to be determined by fitting of the experimental points to the corresponding model. A nonlinear regression procedure is used to minimize the residue Φ, Eq. (7) for TDT and Eq. (22) for CFC, between the experimental values and those stemming from the working equations. The fitting procedure is very demanding due to the need to decompose the time dependence of the measured values into two contributions with quite similar time constants, corresponding to the two eigenvalues of the diffusion matrix. In addition, the fitting is supposed to be performed under the following constraints[9] for the diffusion matrix D_{ij}:

$$\begin{aligned} &D_{11} > 0, \qquad D_{22} > 0, \\ &D_{11}D_{22} - D_{12}D_{21} > 0, \\ &(D_{11} - D_{22})^2 + 4D_{12} \cdot D_{21} \geq 0. \end{aligned} \tag{23}$$

We did not use these inequalities during the fitting procedure, but we applied them to the obtained solutions at different iterative steps, aborting the procedure if Eqs. (23) were not verified. For the system under consideration, the main elements of diffusion matrix resulted were indeed always positive.

Three fitting procedures are available in Matlab, and their combinations have been tested for the processing of the experimental data. The first is an unconstrained Nelder-Mead (simplex) method; the second is a trust region method including its subset, Levenberg-Marquardt (L-M) algorithm; the third is an active set method. All methods display some advantages and disadvantages, useful in some cases and parasitic in others. The simplex method does not require information of an objective function shape or estimation of its gradients. It can explore larger regions in parameter space when looking for the minimum of the objective function. At the same time it becomes less useful when the number of fit parameters is large. It can repeatedly converge to a physically unreasonable result. The trust region method, on the contrary, estimates the shape of an objective function, approximating it by a quadratic surface. This method usually needs less iterations to converge, but only for a good initial guess. With a bad initial guess, it may not converge at all or provide complex values or multiple solutions. Figure 6 shows comparison of fitting convergence applying Levenberg-Marquardt and Nelder-Mead (simplex) algorithms for 70 randomly generated initial guesses. The former provides scattered multiple solutions often almost indistinguishable from initial guess, while the latter always converges to the same point (green). The fitting results are similar for two diffusion couples (D_{11}, D_{12}) and (D_{22}, D_{21}) using experimental results from TDT. We also have tried L-M fitting algorithm by adding analytical calculation of Jacobian. For a large set of tested initial guesses, it works faster and better (no complex solutions) than standard L-M procedure implemented in Matlab with a quadratic approximation for the objective function. However, for the particular system under consideration, it does not find unique solution, and results are similar to that shown in Fig. 6. After testing various procedures, the simplex method was selected as the most suitable for the mixture THN-IBB-nC_{12}. There are multiple local minima of the function Φ in the parameter space D_{ij}, which should be carefully analyzed for selection of the correct solution.

Choice of a reasonable initial guess for iterative methods can lead to a faster convergence. Hence, we divided the modeling process into two steps. The first step is aimed at searching of a good initial guess, and second step is the iterative process to minimize Φ, which uses the initial guess of the first step.

B. Results from the experiments using Taylor dispersion technique

For modeling by Eq. (20) the TDT signals described in Table I, and evaluating the corresponding diffusion coefficients, we used as first step the preliminary fitting runs described in Sec. III C. Hence, as initial guess, the diagonal diffusion coefficients D_{11} and D_{22} are assumed to be equal to the

TABLE III. Diffusion coefficients $D_{ij} \times 10^{10}$, eigenvalues of the diffusion matrix $\hat{D}_i \times 10^{10}$, residual function $\Phi \times 10^3$, $|\delta_{\mathrm{Ons}}|$, and s^2 after 330 iterations of the fitting algorithm, and for five different combinations of the TDT experimental signals reported in Table I. First column specifies the combination used in each case. Last row shows the mean values and standard deviations.

Signals combination	D_{11} (m^2/s)	D_{12} (m^2/s)	D_{21} (m^2/s)	D_{22} (m^2/s)	$\hat{D}_1$ (m^2/s)	$\hat{D}_2$ (m^2/s)	Φ	$\lvert\delta_{\mathrm{Ons}}\rvert$ (%)	s^2
1, 3	10.33	0.21	−4.38	6.62	10.07	6.88	0.90	52	1.041
2, 4	10.31	0.44	−4.38	6.22	9.76	6.77	0.64	55	1.045
1, 2, 3	10.31	0.15	−4.34	6.71	10.12	6.90	0.11	50	1.039
1, 3, 4	10.31	0.54	−4.36	6.07	9.65	6.73	1.36	56	1.046
1, 2, 3, 4	10.32	0.33	−4.37	6.42	9.91	6.83	1.55	53	1.043
	10.31	0.33	−4.36	6.41	9.90	6.82		53	1.042
	±0.01	±0.13	±0.01	±0.21	±0.13	±0.05			

apparent diffusion coefficients D_{app} reported in Table I. The initial guess for the two cross-diffusion coefficients is zero. To obtain information on possible errors during the fitting procedure and on stability of the final solution, we used about 200 initial guesses within 5% margin around the apparent coefficients obtained in the preliminary fitting run.

As already explained, to deduce the diffusion matrix, one has to simultaneously fit at least two experimental signals obtained with different injected samples. To improve the quality of the results, we performed simultaneous fits to different combinations of the available experimental signals reported in Table I. In particular, we fitted two different couples, two different triplets, and the four signals together (up to five different combinations), as specified in the left column of Table III. As required, each combination includes at least one signal from the group 1,2 and one signal from the group 3,4. Then, by the simplex algorithm, we found D_{ij} and the residual value of the objective function Φ for each combination. The results are reported in Table III for the five signal combinations considered. We also report the two eigenvalues of the corresponding diffusion matrix, $\hat{D}_i$, that are independent of the frame of reference. In the last row of Table III, we report the mean $\langle D_{ij} \rangle$ and the corresponding standard deviation of the individual results. The standard deviations (rms) obtained for D_{11} and D_{21} were less than 1%, while for D_{22} was in the range of 3%. The cross-diffusion coefficient D_{12} is one order of magnitude smaller then others, and exhibits a larger standard deviation.

In the last two columns of Table III, we report the Onsager uncertainty $|\delta_{\mathrm{Ons}}|$ and the Hammond's asymmetry index s^2, calculated from the corresponding D_{ij} and G_{ij}, assuming ideal mixture and employing Eqs. (15) and (17), respectively. For the interpretation of these results, we remind that in our case deviations from Onsager symmetry could be not only due to experimental errors in the determination of D_{ij}, but also to deviations of the mixture from ideality.

It is interesting to look at the evolution of the diffusion coefficients and of the Onsager asymmetry $|\delta_{\mathrm{Ons}}|$, from the initial guesses to the final values, as the number of iterations of the simplex minimization algorithm progresses. Figure 7 shows the diffusion coefficients form three plateaus. The existence of the first plateau indicates that the initial guess is quite good. The residual function Φ strongly diminishes after 70 iterations and then remains constant for a while, forming a second plateau, see Fig. 8(a). The solution for D_{ij} on this second plateau is unstable, i.e., strongly depends on the initial guess,

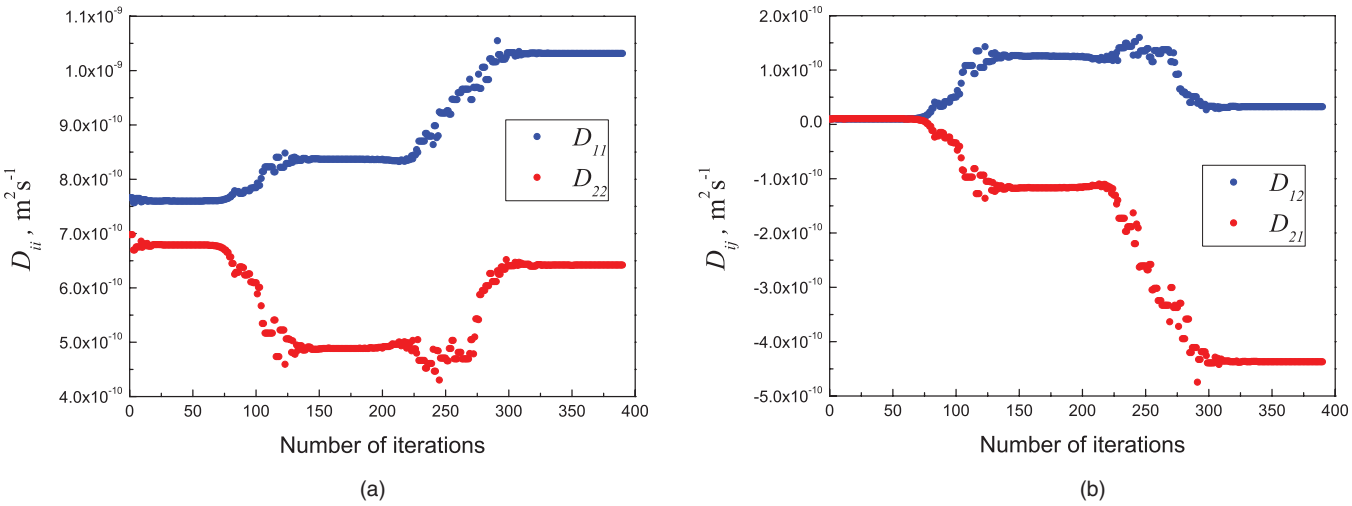

FIG. 7. TDT experiments. Dependence of fit results on the iteration number for (a) main diagonal coefficients and (b) off-diagonal coefficient.

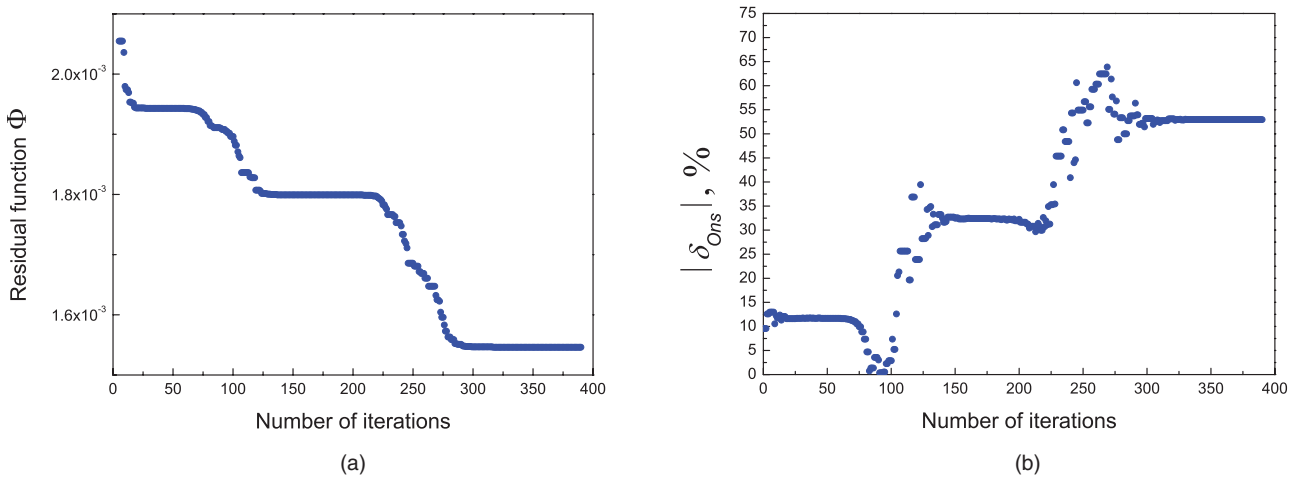

FIG. 8. TDT experiments. (a) Residual function Φ and (b) Onsager asymmetry $|\delta_{Ons}|$ versus number of iterations.

and cannot be considered as final. Indeed, by continuing the iterative process, all the variables under consideration reach a new third plateau at approximately the same step, after about 300 iterations. The solution for the diffusion coefficients on this third plateau does not depend on the initial guesses and is considered as final. The evolution of Onsager asymmetry, $|\delta_{\mathrm{Ons}}|$, is shown in Fig. 8(b). We observe that $|\delta_{\mathrm{Ons}}|$ changes between 150 and 350 iterations, but it has a minimum on the first plateau in the vicinity of 70 iterations.

To finalize this section, we note that besides the standard deviations associated with the fitting procedure, experimental factors like the quality of the Taylor peaks, the baseline subtraction procedure, or the peak time length do contribute to the final error budget. This means that a few percent of systematic errors should be added to the standard deviations reported in the last row of Table III. Related to this systematic error estimation, it should be pointed out that a second series of experiments was performed with liquids with different advertised purity of THN (Sigma-Aldrich, 99%). The results show good reproducibility and the second series is not discussed here. The consistency indicates that the Taylor dispersion technique and the developed analysis procedure constitute a reliable method for the determination of mass diffusion coefficients for this class of liquid mixtures.

C. Results from the experiments using counter flow cell

As already anticipated, in order to obtain good initial guesses for the fitting of the signal $\Delta n(z, t)$ in CFC experiments, we first perform a preliminary modeling pretending that the system is a binary mixture. Mathematically, there is a single concentration in Eq. (21) that evolves in time in accordance to Eq. (5a), with the two exponentials replaced by only one. The quasi-binary diffusion coefficient resulting from this preliminary fake fit was usually close to the smaller eigenvalue of the final D_{ij}, except for CFC experiment #1 where D_{app} was close to the larger eigenvalue. This can be easily understood by referring to Fig. 4, from which it follows that the diffusion couple of experiment #1 is the closest to the larger eigenvector. The diffusion couple of experiment #2 is the closest to the smaller eigenvector, and consequently, it shows the smallest apparent diffusion coefficient.

Next, in a second step, we proceed to the fitting of the experimental signal $\Delta n(z, t)$ to the full model for a ternary system, Eqs. [(5a) and (5b)] and (22). For the complete fit, we adopt the preliminary quasi-binary diffusion coefficient as the initial guess for both D_{11} and D_{22}, while zero is adopted as the initial guess for the cross-diagonal elements of the diffusion matrix.

The simplex minimization algorithm behaves differently in comparison with TDT, and usually the residual function Φ is two orders of magnitude smaller, depending on the level of noise in the experimental data and of course in the number of points contributing to the sum in Eq. (22). Figure 9 shows the variation of the diffusion coefficients with the number of iterations of the simplex minimization algorithm, while Fig. 10(a) shows the evolution of the corresponding residual function Φ, and Fig. 10(b) the evolution of the Onsager uncertainty $|\delta_{\mathrm{Ons}}|$. From a careful examination of Figs. 9 and 10, we conclude that the iterative process in this case does not provide unambiguous results. Obviously, the function Φ has a few local minima. Φ becomes smaller with the number of iterations performed, but at the same time $|\delta_{\mathrm{Ons}}|$ grows.

In summary, we distinguish three different plateaus in all the quantities (D_{ij}, Φ, $|\delta_{\mathrm{Ons}}|$) displayed in Figs. 9 and 10 for the experiments #1 and #4, as well as in similar figures for the other CFC fits that we do not show here. The first plateau continues up to 90–100 iterations. Because the initial guess for the cross-diagonal coefficients was zero, their values at the first plateau are very small and, consequently, $|\delta_{\mathrm{Ons}}|$ is also small (the initial guess for $|\delta_{\mathrm{Ons}}|$ is exactly zero). As a rule, the diffusion coefficients D_{ij} corresponding to this first plateau do not differ much from their initial guesses, and we do not consider this as a realistic solution. After $\simeq$120 iterations, a second plateau forms in all quantities. It is characterized by a small increase in $|\delta_{\mathrm{Ons}}|$ and non-zero cross-diagonal elements, one negative and the other positive. This second plateau is more stable than in the TDT case, and, in principle, we consider it as a better solution than the first plateau.

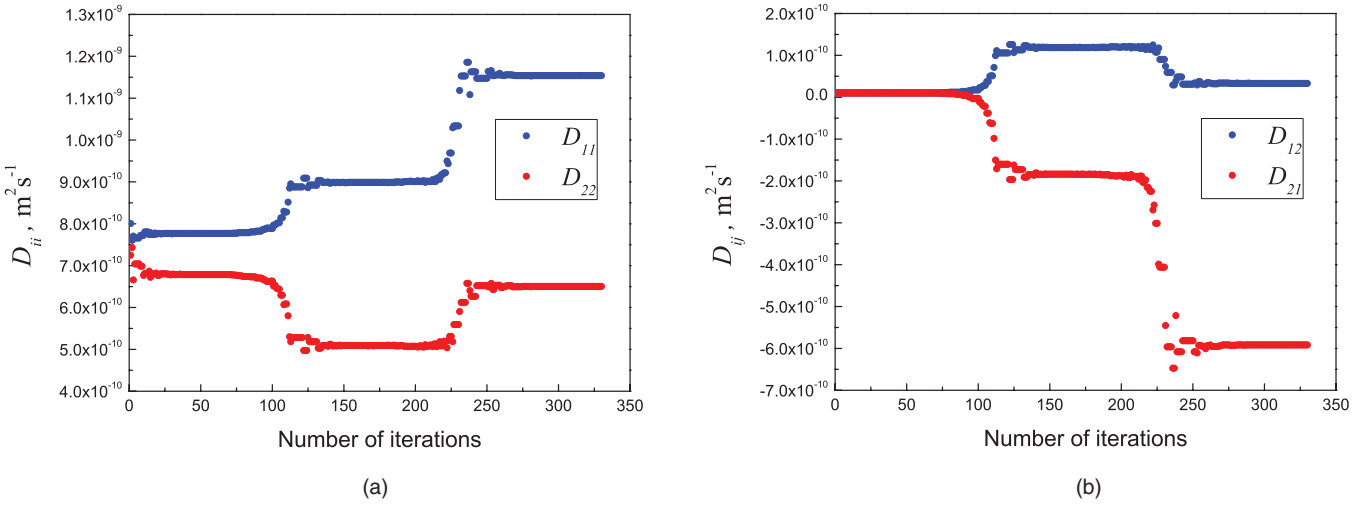

FIG. 9. Counter flow cell. Dependence of fit results on the iteration number for (a) main diagonal coefficients and (b) off-diagonal coefficient.

However, continuation of the iterative process leads to a third plateau, with a significantly smaller value of Φ. In spite of an increment in the Onsager asymmetry $|\delta_{\mathrm{Ons}}|$, we consider this third plateau as the best solution (see below). It should be reminding that our estimations of the Onsager asymmetry rely on the assumption of ideal mixture, Eq. (12). Given the limited information at our disposal about the EOS of our mixture, we quote as final results the values corresponding to this third plateau.

Using the CFC technique, four experiments have been performed with various initial diffusion couples and concentration differences, $\delta c_i(0)$, as shown in Fig. 4. The time evolution of the index of refraction difference between the upper and the lower halves of the cell in the four independent experiments was shown in Fig. 5(a). Obviously, to obtain reliable four diffusion coefficients, we have to simultaneously fit at least two of these experiments. We have combined them into two couples and also the four experiments together, as specified in the left column of Table IV, for simultaneous processing. The evolution of D_{ij}, Φ, and $|\delta_{Ons}|$ with iterations was always similar to the behavior shown in Figs. 9 and 10, that actually corresponds to the (1, 4) experiment combination. The final results (i.e., at the third plateau) for the three combinations of experiments are listed in Table IV. In the last row, we report the mean value and standard deviation (rms) of the three experimental combinations considered. The standard deviations display the same tendency as in the TDT case: rms is the smallest for D_{11} and D_{21} for which it is less than 3%, rms is slightly larger for D_{22} for which it is in the range of 5% and rms is rather large for the cross-diagonal coefficient D_{12}. Earlier publications on diffusion in ternary mixtures also indicated that the standard deviation is large for small cross diffusion coefficients.[22,26] As in the case of TDT, we report in the last two columns of Table IV the Onsager uncertainty $|\delta_{\mathrm{Ons}}|$ and Hammond's asymmetry index s^2 calculated from the corresponding D_{ij} and G_{ij}, assuming ideal mixture and employing Eqs. (15) and (17), respectively.

We conclude this section by reminding the crucial point for this technique: at which plateau to consider the diffusion coefficients as trustworthy? We suggest to consider the values on the third plateau, after 330 iterations, as the better ones. The arguments in favor are: diffusion coefficients do satisfy

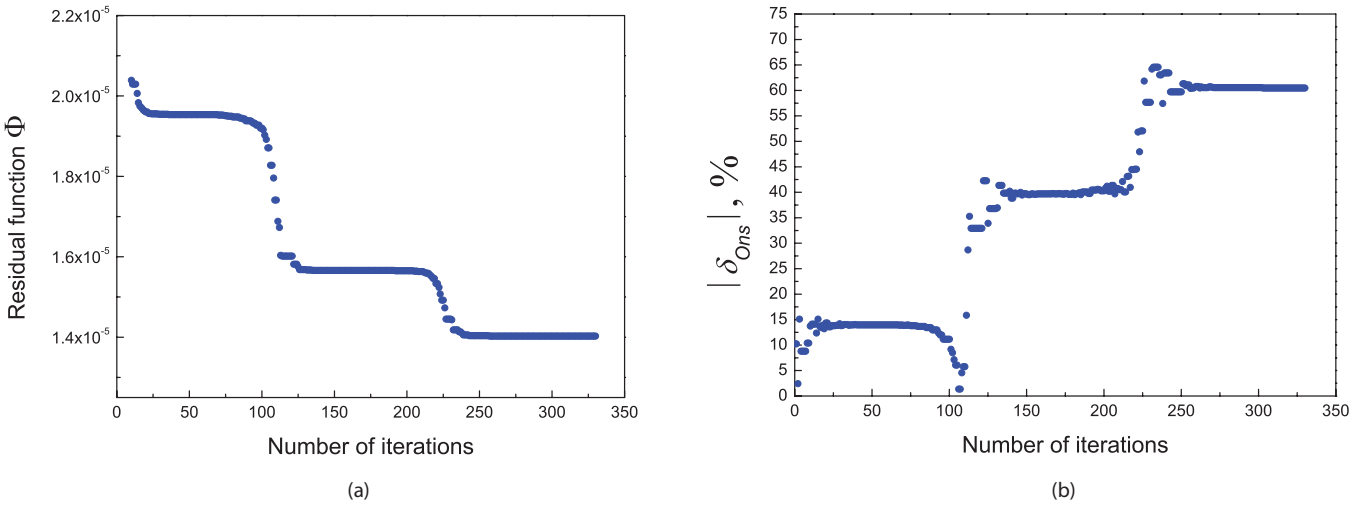

FIG. 10. CFC experiments. (a) Residual function Φ and (b) Onsager asymmetry $|\delta_{\mathrm{Ons}}|$ versus number of iterations.

TABLE IV. The diffusion coefficients $D_{ij} \times 10^{10}$, eigenvalues $\hat{D}_i \times 10^{10}$, residual function $\Phi \times 10^5$, $|\delta_{\mathrm{Ons}}|$, and s^2 after 330 iterations are given for three different combinations of CFC experiments. Last row shows the mean values and standard deviations.

Experiment number	D_{11} (m^2/s)	D_{12} (m^2/s)	D_{21} (m^2/s)	D_{22} (m^2/s)	$\hat{D}_1$ (m^2/s)	$\hat{D}_2$ (m^2/s)	Φ	$\lvert\delta_{\mathrm{Ons}}\rvert$ (%)	s^2
1, 4	11.54	0.34	− 5.91	6.50	11.11	6.93	1.4	60	1.070
2, 3	11.53	0.08	− 6.04	6.82	11.41	7.26	0.87	58	1.068
1, 2, 3, 4	11.70	0.55	− 6.46	6.31	10.99	7.06	2.6	68	1.094
	11.60	0.32	− 6.18	6.65	11.17	7.09		62	1.079
	±0.09	±0.16	±0.19	±0.33	±0.16	±0.19			

Eq. (23), the two main elements are reasonably close to the eigenvalues of the diffusion matrix, and, correspondingly, one of them is close to the apparent (quasi-binary) diffusion coefficient. A possible negative argument would be that asymmetry $|\delta_{\mathrm{Ons}}|$ on the third plateau is higher than on the second plateau. However, one must remember that our current values of $|\delta_{\mathrm{Ons}}|$ also include deviations from an ideal mixture. Only when reliable information about the EOS of our mixture will be available, one can puzzle out this apparent contradiction.

V. DISCUSSION AND COMPARISON WITH AVAILABLE LITERATURE DATA

The literature on mass diffusion in ternary mixtures of hydrocarbons is very limited. For the symmetric point of our same mixture, diffusion coefficients were measured by Königer *et al.*[9] using an optical beam deflection (OBD) technique, which is based on low-profile Soret cell and where diffusion coefficients are measured by fitting kinetics of thermodiffusion separation. Open capillary technique has been used for the determination of mass diffusion coefficients for the mixture octane-decane-1-methylnaphthalene with equal mass fractions.[2] Other investigators attempted to use a sliding symmetric tubes technique,[37] but the number of the experiments performed was insufficient to arrive at decisive conclusions. We have published earlier pioneering measurements of mass diffusion coefficients in ternary mixtures of hydrocarbons[27,33] for which the fine-tune described in Secs. III C and III E was not performed. Consequently, they are not comparable with our present results and we do not further analyze them here. Regarding non-hydrocarbon ternary liquid mixtures, there exist several recent experimental investigations,[3–7] due to the different nature of the system they also are not comparable with our present results.

In ternary mixtures the numerical values of the Fickian diffusion matrix depend on the order of the components. The coefficients D^*_{ij} determined for our same mixture elsewhere by OBD[9] are reported with the component order: nC_{12}-IBB-THN (c^*_1, c^*_2, c^*_3), while in present work the order THN-IBB-nC_{12} (c_1, c_2, c_3) was preferred. Hence, we have to change component order to compare the available literature data[9] with our present results. Equations (1) and (2) for the mass fluxes in variables (c_1, c_2, c_3) can be rewritten in vector form as

$$\mathbf{J}_i = -\rho_0 D_{ij} \nabla c_j.$$

The relation with the superscript * variables ($c_1 = 1 - c^*_1 - c^*_2$, c_2, $c_3 = c^*_1$) can be expressed via

$$\mathbf{J}_i = Q_{ij}\mathbf{J}^*_j, \quad \nabla c_i = Q_{ij}\nabla c^*_j, \quad \mathsf{D} = \mathsf{Q}\mathsf{D}^*\mathsf{Q}^{-1}, \tag{24}$$

where D is the diffusion matrix and Q is the matrix with elements $Q_{ij} = \partial c_i / \partial c^*_j$. In our case,

$$\mathsf{Q} = \begin{pmatrix} -1 & -1 \\ 0 & 1 \end{pmatrix}. \tag{25}$$

Then the diffusion coefficients D_{ij} for the order THN-IBB-nC_{12} are related to the diffusion coefficients D^*_{ij} for the order nC_{12}-IBB-THN by

$$\begin{aligned} D_{11} &= (D^*_{11} + D^*_{21}), \\ D_{12} &= (D^*_{11} - D^*_{22} + D^*_{21} - D^*_{12}), \\ D_{21} &= -D^*_{21}, \\ D_{22} &= D^*_{22} - D^*_{21}. \end{aligned} \tag{26}$$

All the results for the symmetric point of the mixture THN-IBB-nC_{12} are summarized in Table V. The first observation is that all techniques provide similar eigenvalues: $\hat{D}_1 = 10.6 \times 10^{-10}$ m^2 s^{-1} and $\hat{D}_2 = 6.88 \times 10^{-10}$ m^2 s^{-1}, with standard deviations of 5% and 2%, respectively. However, OBD results for D_{ij} do not seem to agree with the other techniques. It looks as if the indices have been exchanged in OBD results. Indeed, by formal exchange of "1" by "2" in the OBD results of Table V, all three techniques will provide similar results: largest coefficients is D_{11}, smallest and positive is D_{12}, while the second off-diagonal element D_{21} is relatively large and negative, similar in order of magnitude (although of different sign) to the second main element D_{22}. On the one hand, we do not have an explanation for the disagreement in D_{ij}, other than the intrinsic difficulty of measuring diffusion

TABLE V. Summary of available results for symmetric point of THN-IBB-nC_{12} mixture: mass diffusion coefficients $D_{ij} \times 10^{10}$, eigenvalues $\hat{D}_i \times 10^{10}$, and $|\delta_{\mathrm{Ons}}|$.

	D_{11} (m^2/s)	D_{12} (m^2/s)	D_{21} (m^2/s)	D_{22} (m^2/s)	$\hat{D}_1$ (m^2/s)	$\hat{D}_2$ (m^2/s)	$\lvert\delta_{\mathrm{Ons}}\rvert$ (%)	s^2
TDT	10.31	0.33	− 4.36	6.41	9.9	6.82	53	1.042
CFC	11.60	0.32	− 6.18	6.65	11.17	7.09	63	1.079
OBD[9]	5.62	− 5.91	1.08	12.18	10.99	6.81	66	1.077

matrices in ternary systems. On the other hand, the fact that the eigenvalues are similar for the three data-sets is understandable because they are directly obtained from the fittings, while to obtain the four components of the diffusion matrix requires extra information and, thus, is more sensible to error.

We took an advantage of good agreement between eigenvalues obtained from all the techniques to make an additional cross-check of our results. Considering eigenvalues $\hat{D}_1$ and $\hat{D}_2$ of diffusion matrix as known, the only two elements of diffusion matrix remain free. Assume that the D_{11} and D_{12} are unknown. Then D_{21} and D_{22} are dependent and can be expressed via sum and multiple of eigenvalues as

$$D_{22} = \hat{D}_1 + \hat{D}_2 - D_{11}, \qquad D_{21} = \frac{D_{11}\, D_{22} - \hat{D}_1\, \hat{D}_2}{D_{12}}. \tag{27}$$

The experimental data were re-processed with two-parameters fit which should be much more robust. All these fits consistently resulted in large D_{11} value, confirming correctness of our four-parameters fit.

The approach of known eigenvalues gives a unique opportunity to visualize a landscape of objective (residual) function of two variables, (D_{11}, D_{12}), in considered case. The presented map in Fig. 11 has a set of interesting features worth discussing. First of all, the objective function is definitely of the ravine (or valley) type. It means that accuracy of solution can be rather low along direction of the valley. Second, the map is marked out not only by presence of ravines, but also by ridge of local maxima, separating them. Existence of this ridge can partially explain why optimization techniques based on a gradient calculation or on a calculation of a local shape of the residual function fail in such situation: they probably cannot overcome such ridge, and so, will strongly depend upon location of initial guess. The topology of the residual function is similar for TDT and CFC techniques, and in Fig. 11 only the results for CFC technique are presented.

This can also explain discrepancy between present results and work by Königer *et al.*[9] Figure 11 shows that our solution is located on north of the ridge, in region with positive D_{12}, while another one got stuck southward of the ridge being probably attracted by another valley. It should be noted that our previously reported results[33] correspond to a local minimum (yellow circle in Fig. 11). To finalize the discussion, we have to note that the general view of such maps is similar for any possible combinations of two independent diffusion coefficients. Furthermore, the variations of eigenvalues within the experimental range provide only a fine-tuning of the map, but not a fundamental change that may indicate something specific to diffusion problem in general.

The Onsager uncertainty $|\delta_{\mathrm{Ons}}|$ of Eq. (15) and the Hammond's asymmetry index of Eq. (17), calculated under the assumption of ideal mixture, are given for each data set in the last two columns of Table V. We observe that these parameters are similar for all techniques, although TDT seems to give slightly better results. The values of s^2 indicate a moderate asymmetry in DG^{-1} that we interpret as likely due to experimental errors and uncertainty in the equilibrium EOS. We do not observe a clear violation of the Onsager reciprocal relations for any data set, so that we do not consider this test to be accurate enough to reject any of the reported D values. It is worth recalling here that $|\delta_{\mathrm{Ons}}|$ depends on the order of components, while s^2 does not. For example, if $|\delta_{\mathrm{Ons}}|$ were calculated from the original OBD data,[9] i.e., for the component order nC_{12}-IBB-THN, it would result in $|\delta_{\mathrm{Ons}}| = 76\%$, instead of the value 66% quoted in Table V. However, the s^2 value is the same in the two cases. Hence, it is preferable to make statements about Onsager reciprocal relations based on s^2 rather than on $|\delta_{\mathrm{Ons}}|$.

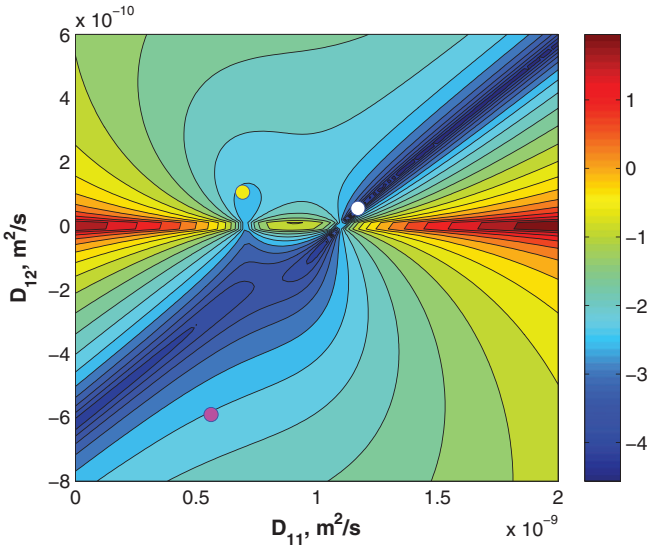

FIG. 11. Topology of residual function Φ (in logarithmic scale with base 10) against two unknown parameters D_{11} and D_{12} at fixed eigenvalues. The residual function is calculated for four runs of CFC with eigenvalues $\hat{D}_i$ from Table IV. White dot indicates results from CFC technique in this paper, while yellow point indicates our previously reported results;[33] pink dot indicates solution in Ref. 9.

VI. CONCLUSIONS

We have measured the Fickian diffusion coefficients for a ternary liquid mixture with equal mass fractions of THN, IBB, and nC_{12} at the constant temperature of $T = 298$ K and at atmospheric pressure. The ternary mixtures of these compounds are currently under investigation as model systems for truly hydrocarbon multicomponent mixtures, and this same system has also been chosen as the first system for microgravity experiments in the DCMIX project.[18] Since experiments with ternary mixtures are much more complicated and error prone than equivalent measurements in binaries, two different techniques were adopted: Taylor dispersion and counter flow cell. The results from both instruments show the reliability of obtaining both the diagonal and the cross-diagonal diffusion coefficients in ternary mixtures by these methods. The main diagonal elements are positive and the eigenvalues of the ternary mixture are close to the pseudo-binary diffusion coefficients. Our eigenvalues agree reasonably with literature data of Königer *et al.*,[9] although the individual components of the diffusion matrix are somewhat different.

To further the reliability of the reported diffusion matrices, we have checked how well they verify the Onsager re-

ciprocal relations. This goal has been somehow compromised because of the lack of the information on the equilibrium EOS of this particular mixture, which leads us to adopt an ideal mixture approximation. For a quantitative assessment of the verification of Onsager relations, we propose to use the Hammond's asymmetry index, s^2, that is particularly well-suited for this purpose, since the s^2 associated to an experimental data set is independent of the frame of reference, or the order in which the components are listed in the mixture (see Sec. V). Unfortunately, the results of the Onsager analysis are rather inconclusive, and just show that more effort will be required in the future to turn this analysis into a really useful tool for diffusion research. In particular, teamwork with an experimental group expert in the measurement of equilibrium EOS may be required.

In the future, we plan to extend the experimental techniques and mathematical approaches developed in this work to ternary mixtures with the same components: THN, IBB, and nC_{12}, but over the entire concentration range.

ACKNOWLEDGMENTS

This work is supported by the PRODEX programme of the Belgian Federal Science Policy Office, ESA. The authors would like to thank referee for useful discussion of the fitting algorithms.

[1]M. M. Bou-Ali and J. K. Platten, J. Non-Equilib. Thermodyn. **30**, 385 (2005).
[2]A. Leahy-Dios, M. M. Bou-Ali, J. K. Platten, and A. Firoozabadi, J. Chem. Phys. **122**, 234502 (2005).
[3]D. A. Ivanov, Th. Grossmann, and J. Winkelmann, Fluid Phase Equilib. **228–293**, 228 (2005).
[4]A. C. F. Ribeiro, J. C. S. Gomes, M. C. F. Barros, V. M. M. Lobo, and M. A. Esteso, J. Chem. Thermodyn. **43**, 270 (2011).
[5]D. A. Ivanov and J. Winkelmann, Int. J. Thermophys. **29**, 1921 (2008).
[6]T. Grossmann and J. Winkelmann, J. Chem. Eng. Data **54**, 405 (2009).
[7]T. Grossmann and J. Winkelmann, J. Chem. Eng. Data **54**, 485 (2009).
[8]P. Blanco, M. M. Bou-Ali, J. K. Platten, D. A. de Mezquia, J. A. Madariaga, and C. Santamaría, J. Chem. Phys. **132**, 114506 (2010).
[9]A. Königer, H. Wunderlich, and W. Köhler, J. Chem. Phys. **132**, 174506 (2010).
[10]V. Sechenyh, J. C. Legros, and V. Shevtsova, J. Chem. Eng. Data **57**, 1036 (2012).
[11]A. Bardow, Fluid Phase Equilib. **251**, 121 (2007).
[12]J. M. Ortiz de Zárate, J. L. Hita, and J. V. Sengers, C. R. Mec. **341**, 399 (2013).
[13]H. T. Cullinan, Jr., Ind. Eng. Chem. Fundam. **4**, 133 (1965).
[14]J. W. Mutoru and A. Firoozabadi, J. Chem. Thermodyn. **43**, 1192 (2011).
[15]A. Mialdun, V. Yasnou, V. Shevtsova, A. Königer, W. Köhler, D. A. de Mezquia, and M. M. Bou-Ali, J. Chem. Phys. **136**, 244512 (2012).
[16]M. Gebhardt, W. Köhler, A. Mialdun, V. Yasnou, and V. Shevtsova, J. Chem. Phys. **138**, 114503 (2013).
[17]G. B. Ray and D. G. Leaist, J. Chem. Eng. Data **55**, 1814 (2010).
[18]A. Mialdun, C. Minetti, Y. Gaponenko, V. Shevtsova, and F. Dubois, Microgravity Sci. Technol. **25**, 83 (2013).
[19]R. Taylor and R. Krishna, *Multicomponent Mass Transfer* (Wiley, 1993).
[20]S. R. de Groot and P. Mazur, *Non-Equilibrium Thermodynamics* (Dover, 1984).
[21]V. Shevtsova, V. Sechenyh, A. Nepomnyashchy, and J. C. Legros, Philos. Mag. **91**, 3498 (2011).
[22]F. J. Spera and A. F. Trial, Science **259**, 204 (1993).
[23]G. I. Taylor, Proc. R. Soc. London, Ser. A **219**, 186 (1953).
[24]W. E. Price, J. Chem. Soc., Faraday Trans. 1 **84**(7), 2431 (1988).
[25]A. Alizadeh, C. A. N. de Castro, and W. A. Wakeham, Int. J. Thermophys. **1**(3), 243 (1980).
[26]V. K. Vanag, F. Rossi, A. Cherkashin, and I. R. Epstein, J. Phys. Chem. B **112**, 9058 (2008).
[27]V. Sechenyh, J. C. Legros, and V. Shevtsova, C. R. Mec. **341**, 490 (2013).
[28]V. Sechenyh, J. C. Legros, and V. Shevtsova, J. Chem. Thermodyn. **62**, 64 (2013).
[29]J. H. Hammond, "Solving asymmetric variational inequalities and systems of equations with generalized nonlinear programming algorithms," Ph.D. thesis, MIT, Boston, 1984.
[30]G. Perakis, Math. Op. Res. **32**, 614 (2007).
[31]Ph. W. M. Rutten, "Diffusion in Liquids," Ph.D. thesis, Delft University, Delft, The Netherlands, 1992.
[32]J. F. Torres, A. Komiya, E. Shoji, J. Okaji, and S. Maruyama, Opt. Lasers Eng. **50**, 1287 (2012).
[33]A. Mialdun, V. Yasnou, and V. Shevtsova, C. R. Mec. **341**, 462 (2013).
[34]A. Mialdun and V. Shevtsova, J. Chem. Phys. **134**, 044524 (2011).
[35]A. Mialdun and V. Shevtsova, C. R. Mec. **339**, 362 (2011).
[36]M. S. Thompson and J. E. Morral, Acta Metall. **34**, 339 (1986).
[37]M. Larrañaga, M. M. Bou-Ali, D. Soler, M. Martinez-Aguirre, A. Mialdun, and V. Shevtsova, C. R. Mec. **341**, 356 (2013).